ACS OMEGA

http://pubs.acs.org/journal/acsodf

Article

Effects of Composite Accelerators on the Formation of Carbon Dioxide Hydrates

Yingmei Wang,* Aili Niu, Shenghao Liu, Ji Chen, Xuemin Zhang, and Jing Zhan

Cite This: *ACS Omega* 2022, 7, 15359−15368

Read Online

ACCESS | Metrics & More | Article Recommendations

ABSTRACT: To improve the rate of formation of carbon dioxide hydrates, tetra-*n*-butylammonium bromide (TBAB) was compounded with different concentrations of sodium dodecyl sulfate (SDS) and nanographite, and the effects of these mixtures on carbon dioxide hydrate formation were studied. The addition of TBAB alone, as well as mixtures of TBAB and SDS or nanographite, shortened the induced nucleation time, and the induction times of the TBAB−2.5 g/L nanographite and TBAB−0.24 g/L SDS systems were the shortest and longest, respectively. Further, on mixing TBAB and SDS, the induced nucleation time first increased and then decreased with the increase in the SDS concentration. When TBAB and nanographite were mixed together, the induced nucleation time first decreased, then increased, and again decreased with the increase in the nanographite concentration. In addition, the hydrate formation rate and conversion were highest for the TBAB−0.48 g/L SDS system and lowest for the TBAB−0.06 g/L SDS system; in the first 35 min, from the end of gas charging, the TBAB−10 g/L nanographite and TBAB−5 g/L nanographite systems yielded the highest and lowest hydrate formation rates and conversions, respectively. For the composite systems, obvious effects were observed in the initial stages of reaction, but the effects varied over the course of the reaction. Overall, the use of different accelerators resulted in little differences in the total production, conversion, and formation rate of carbon dioxide hydrates over the course of the reaction.

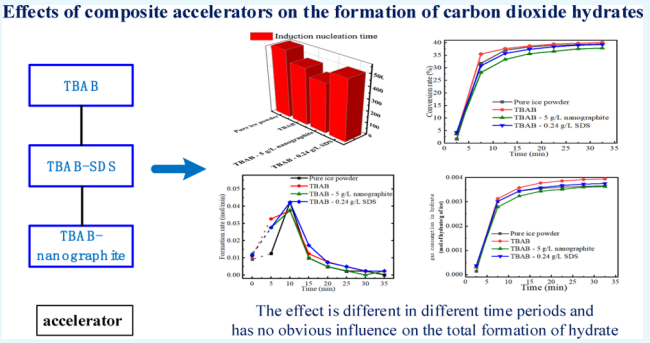

1. INTRODUCTION

Natural gas hydrate technology has been widely used in gas storage and transportation,[1] seawater desalination,[2] CO_2 storage,[3] cold-storage technology,[4] and transportation; however, owing to the slow hydrate formation rate and low gas storage capacity, its large-scale industrial utilization has been limited.[5,6] Therefore, researchers have focused on increasing the rate of hydrate generation.[6−9] Physical and chemical methods can be used to increase this rate. Physical methods involve expanding the gas−liquid contact area and enhancing the heat- and mass-transfer capacity[10] by bubbling,[11] stirring,[12] or spraying.[13] In contrast, in the chemical method, the formation of hydrates is enhanced by adding accelerators, which allow the use of milder reaction conditions and increase the amount of dissolved gas.[14−16] Concerning energy consumption and cost, physical methods are less favorable than chemical methods, so chemical methods have proven to be popular. Common accelerators include thermodynamic accelerators,[17] kinetic accelerators,[18] nanofluids,[19] ionic accelerators,[20] biosurfactants, and others.[21,22] Among them, surfactants and kinetic accelerators have attracted the most attention because they show the best enhancement of hydrate formation.[23−25]

For example, Ye et al.[26] found that the addition of tetra-*n*-butylammonium bromide (TBAB) in mass fractions of 0.1 and 0.05 accelerates the rate of formation of carbon dioxide hydrates, and the addition of 0.05 wt % TBAB was optimal. Babu et al.[27] tested the effect of the addition of 0.3, 1, 1.5, 2, and 3 mol % TBAB and found that the 1 mol % TBAB solution resulted in the highest rate of carbon dioxide hydrate formation. Further, the induction time when using the 0.3 mol % TBAB solution was the longest, and the overall gas consumption was the largest because this solution had high gas solubility before nucleation. Nguyen et al.[28] found that the use of a solution containing 0.125% TBAB reduced the carbon dioxide hydrate formation rate, thus acting as an inhibitor. Therefore, accelerators can show different effects on the hydrate formation rate at different concentrations. Further, for a single accelerator, there is an optimal concentration, but this concentration changes with temperature, pressure, and other factors.

Received: December 3, 2021
Accepted: March 30, 2022
Published: April 29, 2022

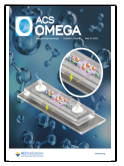

Table 1. Effects of TBAB, SDS, Nanographite, and Other Accelerators on Hydrate Formation

author	year	temperature (K)	pressure	accelerator	gas
Ye et al.[26]	2014	286.83, 289.06	4.03 MPa	0.05 and 0.10 wt % TBAB	CO_2
Babu et al.[27]	2014	279.2	6 MPa	0.3, 1.0, 1.5, 2.0, and 3.0 mol % TBAB	CO_2
Nguye et al.[28]	2016	274.65	2.65 MPa	0−3 wt % TBAB	CO_2
Mech et al.[30]	2016	276.15	7.5 MPa	0.05 wt % TBAB and 600 ppm SDS	CO_2
Zhou et al.[31]	2018	276.45	3.8 MPa	9.01 wt % TBAB and 0.04, 0.06, or 0.08 wt % nanographite	CO_2
Babaee et al.[32]	2018	281, 285, and 287.5	6.1, 8.1, and 10.1 MPa	0.1, 0.3 wt % TBAB and 100 or 200 ppm SDS	CO_2
Sarlak et al.[33]	2019	274.15, 276.15, and 278.15	36, 38, and 40 bar	1, 3, and 5 wt % TBAB and 500 ppm SDS	CO_2
Zhang et al.[29]	2021	283.15	3.8 MPa	10 wt % TBAB and 0−1500 ppm SDS	70% CO_2 + 30% N_2

Zhang et al.[29] studied the effects of TBAB combined with 0.05, 0.1, and 0.15 wt % sodium dodecyl sulfate (SDS) on the induced nucleation time and the yield of carbon dioxide hydrate at 276.45 K and 3.8 MPa and found that this combination of accelerators shortened the induced nucleation time to a greater extent than using TBAB alone. In addition, hydrate formation increased with an increase in undercooling when 10 wt % TBAB and 0.05 wt % SDS were used. In contrast, Mech et al.[30] found that the hydrate conversion when using 0.05 wt % TBAB and 600 ppm SDS was less than that of TBAB alone at 5.5 MPa and 276.15 K, but, at 7.5 MPa and 276.15 K, the hydrate formation rate of this system in the initial 3 h was greater than that of TBAB alone. In addition, the hydrate conversion rate of this system was greater than that containing 0.05 wt % TBAB and 1000 ppm SDS, but the use of both systems resulted in lower conversions than using TBAB alone after the initial 3 h. Zhou et al.[31] studied the effect of the combination of 9.01 wt % TBAB and 0.04, 0.06, and 0.08 wt % nanographite on the formation of carbon dioxide hydrate (Table 1). The results showed that the combination of TBAB and 0.08 wt % nanographite resulted in the highest hydrate formation rate and the highest conversion and, thus, the best overall performance.

Therefore, to date, many studies on the effects of single and compound accelerators on hydrate formation have been published. Different kinds of accelerators have different effects when they are mixed. Further, the effects of an accelerator on hydrate formation differ at different concentrations and with different accelerator combinations. Therefore, it is necessary to study the effects of different accelerator types and concentrations on carbon dioxide hydrate formation and identify the optimal combinations and concentrations. Previous research has shown that mixtures of SDS, TBAB, and nanographite can enhance the formation of carbon dioxide hydrates compared to the use of SDS and nanographite alone; therefore, in this study, using the optimal TBAB concentration (vide infra), we studied the effects of different concentrations of SDS and nanographite on carbon dioxide hydrate formation at 272.65 K and 3.3 MPa. In detail, Babu et al.,[27] Zhou et al.,[34] and Lin et al.[35] found that the optimum concentrations of TBAB, nanographite, and SDS for carbon dioxide hydrate formation to be 0.288, 5, and 0.24 g/L respectively, so TBAB was combined with 0.06, 0.12, 0.24, 0.36, or 0.48 g/L SDS or 1.25, 2.5, 5, 7.5, and 10 g/L nanographite. Thus, we identified the most suitable accelerator system for enhancing carbon dioxide hydrate formation. The findings of this study will aid the industrialization of carbon dioxide hydrate formation and the rapid capture of carbon dioxide, thus enabling the large-scale utilization of hydrates.

2. EXPERIMENTAL SECTION

2.1. Materials. CO_2 was provided by Lanzhou Zhongkekate Co. Ltd. (purity: 99.99%). Deionized water was prepared in our laboratory and had a conductivity of 18.25 m Ω cm. SDS was provided by Chuang Baiyou Biological Reagent Consumables (purity: 99.9%). Nanographite was provided by Jishengya Nano Technology Co. Ltd. (10,000 mesh; purity: 99.9%). TBAB was provided by Shanghai McLean Biochemical Technology Co. Ltd. and had a purity of 99.9%.

2.2. Apparatus. The experimental system used in this experiment is shown in Figure 1 (yellow represents the circuitry and black represents the gas pipeline). The experimental device consisted of two stainless-steel reactors and a circulating cold bath, vacuum pump, data acquisition instrument, precooling tank, refrigeration device, and computer. The internal volume of a single reactor was 605 mL, and the maximum pressure limit was 20 MPa. To maintain a constant temperature, the hydrate reactor was immersed in a constant-temperature circulating cold bath containing absolute ethanol. The refrigeration device was used to precool the gas in the precooling tank to reduce ice melting. An Agilent data acquisition instrument with an accuracy of ±0.05 °C was used to monitor the temperature in the reactor and the circulating cold bath temperature and record and display these values online. The pressure in the reactor was measured and recorded using an SWP pressure sensor [(−1 to 20 ± 0.01) MPa].

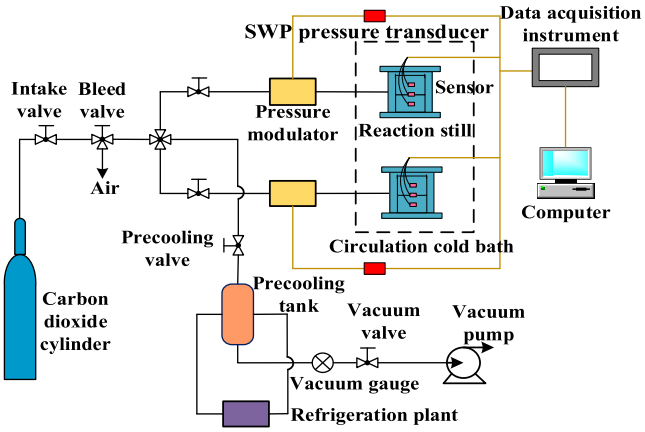

Figure 1. Carbon dioxide hydrate formation apparatus.

2.3. Procedures. Carbon dioxide hydrate was produced using the constant temperature method. Before the experiment, the beaker and reactor were cleaned with deionized water at least three times and dried. Then, TBAB (0.288 g) was evenly mixed with SDS (0.06, 0.12, 0.24, 0.36, or 0.48 g) or nanographite (1.25, 2.5, 5, 7.5, or 10 g) and 1000 mL of water. Once all components were dissolved and mixed homogeneously, the mixture was frozen and ground into ice powder. The particle size of the powder was 0.5−1 mm. Then, the powdered sample (87.9 g) was placed into the frozen reactor. The sample was filled to

https://doi.org/10.1021/acsomega.1c06834
ACS Omega 2022, 7, 15359−15368

the same height each time to ensure that the same sample volume was used. The reactor and sensor were then installed, and the temperature of the circulating cold bath was adjusted to 272.65 K. Simultaneously, vacuum was applied to the solution for 10 min. After reaching the set temperature, the precooled gas was charged into the reactor to 3.3 MPa to initiate hydrate formation. The hydrate formation process was considered to have been completed when the pressure and temperature in the reactor did not vary for 48 h after the formation of the carbon dioxide hydrate.

2.4. Data Processing. The amount, rate, and conversion of carbon dioxide hydrate were considered during analysis and experiment. The calculation process is as follows.

2.4.1. Amount of Generated Carbon Dioxide Hydrate. The amount of carbon dioxide hydrate formed was determined at different periods of the experiment: during the gas charging process and from the end of gas charging to the end of the experiment. The amount of hydrate generated during gas charging gas charging, n_f, is the difference between that produced over the entire experiment (beginning to the end of the experiment) and that generated from the end of gas charging to the end of the experiment, as given by eq 1.

$$n_f = n_d - n_e \tag{1}$$

Here, n_f, n_d, and n_e are the amounts of hydrate generated during gas charging, over the entire experiment, and from the end of gas charging to the end of the experiment (mol), respectively.

The percentage of volume generated during gas charging with respect to the whole generated volume is given by eq 2.

$$\eta_{f1} = \frac{n_f}{n_d} \times 100\% \tag{2}$$

Here, η_{f1} is the percentage of volume generated during gas charging with respect to the whole generated volume.

Using the experimental temperature and pressure and the equation for hydrate formation, the amount of hydrate in the reactor from the end of gas charging to the end of the experiment, n_e, was calculated, as shown in eq 7.

$$n_h H_2O + CO_2 = CO_2 \cdot n_h H_2O \tag{3}$$

Here, n_h is the hydration number. The amount of TBAB used was 8.93×10^{-4} mol, and the amount of carbon dioxide hydrate generated by the final TBAB system is 0.3457 mol; thus, the TBAB accounts for 2.58‰ of the final amount of hydrate. Because of this low value, the semi-cage hydrate generated by TBAB and pure ice powder was ignored, and the hydration number was assumed to be 5.75[36] under ideal conditions.

$$n_o = \frac{P_o V}{Z_o R T_o} \tag{4}$$

Here, P_o and T_o are the pressure (MPa) and temperature (K), respectively, in the reactor at the end of inflation, V is the volume (L) occupied by the gas in the reactor at the end of inflation, R is the universal gas constant (8.314 J/(mol K)), Z_o is the gas compression factor at the end of inflation, which was obtained by iteration of the Peng−Robison (PR) equation calculated by Li et al.[37] and Smith,[38] and n_o is the amount of carbon dioxide hydrate in the reactor at the end of inflation.

The amount of carbon dioxide hydrate in the reactor from the end of inflation to the end of the formation experiment, n_t, was calculated using eq 5.

$$n_t = \frac{P_t V}{Z_t R T_t} \tag{5}$$

Here, P_t and T_t are the pressure (MPa) and temperature (K), respectively, at time t from the end of inflation to the end of the experiment, and Z_t is the gas compression factor at time t from the point when gas charging stopped to the end of the experiment; this was also obtained using the PR equation reported by Li et al.[37] and Smith.[38] Finally, n_t is the amount of carbon dioxide hydrate in the reactor at time t from when gas charging stopped to the end of the generation experiment.

Therefore, the amount of carbon dioxide hydrate generated at any time from the end of charging to the end of the experiment, Δn, is given by eq 6.

$$\triangle n = n_o - n_t = \frac{P_o V}{Z_o R T_o} - \frac{P_t V}{Z_t R T_t} \tag{6}$$

The generation amount from the end of inflation to the end of the experiment, n_e, was calculated, as shown in eq 7.

$$n_e = n_o - n_1 = \frac{P_o V}{Z_o R T_o} - \frac{P_1 V}{Z_1 R T_1} \tag{7}$$

Here, P_1 and T_1 are the pressure (MPa) and temperature (K) at the end of the generation experiment, respectively, and Z_1 is the gas compression factor at the end of the generation experiment, which was obtained using the PR equation as proposed by Li et al.[37] and Smith.[38] n_1 is the amount of carbon dioxide hydrate in the reactor at the end of the generation experiment.

2.4.2. Rate of CO_2 Hydrate Formation. The average rate of carbon dioxide hydrate formation was assessed during the gas charging process and from the beginning of gas charging to the end of the formation experiment. The formation rate during the charging process, v_f, is the ratio of the amount of carbon dioxide hydrate generated during charging from the beginning of induced nucleation to the end of charging, as given by eq 8.

$$v_f = \frac{n_f}{t_f} \tag{8}$$

Here, v_f has units of mol/min and t_f is the time from the beginning of induced nucleation time to the end of inflation (min).

The formation rate[38] from the end of gas charging to the end of the experiment was calculated every 5 min. Using eq 8, the average formation rate of carbon dioxide hydrate every 5 min (v) can be calculated.

$$v = \frac{n_i - n_{i+5}}{5} \qquad (i = i + 5,\ i = 0) \tag{9}$$

Here, n_i is the amount of carbon dioxide hydrate in the reactor from the end of gas charging to i min and to the end of the experiment and n_{i+5} is the amount of carbon dioxide hydrate in the reactor at $i + 5$ min.

2.4.3. Ice Conversion Rate. The ice conversion rate is the ratio of ice consumed before and after the reaction to the amount of ice in the reactor during the experiment. In this study, we investigated the conversion rate during the gas charging process and that from the end of gas charging to the end of the experiment. The conversion rate, η_f, during gas charging is the difference between the conversion rate from the beginning to the end of the experiment, η_d, and that from the beginning of gas charging to the end of the experiment, η_g, as given by eq 13.

https://doi.org/10.1021/acsomega.1c06834
ACS Omega 2022, 7, 15359−15368

Table 2. Composite Systems, Hydrate Generation, Percentage Generation, and Conversion

case	accelerator	generation during gas charging (mol)	percentage of total generation %	conversion during gas charging %	standard deviation during gas charging	standard deviation of induced nucleation time
1	pure ice powder	0.0865	20	10.49	0.0011	1.2374
2	TBAB	0.0924	21.09	10.88	0.0177	2.4749
3	TBAB−0.006 wt % SDS	0.0722	17.6	8.5	0.0077	4.5962
4	TBAB−0.012 wt % SDS	0.0304	8.21	3.58	0.0071	2.1213
5	TBAB−0.024 wt % SDS	0.0936	21.53	11.02	0.0008	1.0783
6	TBAB−0.036 wt % SDS	0.0405	10.76	4.77	0.0147	2.0329
7	TBAB−0.048 wt % SDS	0.1174	22.67	21.51	0.0168	1.0607
8	TBAB−0.125 wt % nanographite	0.069	17.05	8.12	0.0107	2.1213
9	TBAB−0.25 wt % nanographite	0.088	20.86	10.36	0.0028	0.3536
10	TBAB−0.478 wt % nanographite	0.086	17.52	10.13	0.0175	1.5910
11	TBAB−0.72 wt % nanographite	0.0841	19.92	9.9	0.0013	1.7678
12	TBAB−0.99 wt % nanographite	0.0613	17.78	7.22	0.0054	1.2374

$$\eta_f = \eta_d - \eta_g \quad (10)$$

The total conversion rate η_d is calculated based on the measured total production, that is, conversion rate η_g from the beginning to the end of the experiment and is given by eq 11.

$$\eta_d = \frac{5.75 n_d}{n_s} \quad (11)$$

The conversion rate at any time from the stop of inflation to the end of the generation experiment, $\Delta\eta$, is given by eq 12.

$$\Delta\eta = \frac{5.75 \Delta n}{n_s} \quad (12)$$

In addition, eq 13 provides the conversion rate from the end of gas charging to the end of the experiment

$$\eta_g = \frac{5.75 n_e}{n_s} \quad (13)$$

Here, as above, n_s is the amount of ice in the reactor and η_g is the ice conversion rate.

3. RESULTS AND DISCUSSION

3.1. Determination of the Induction Period and Hydrate Formation Phase. To enable the comparison of the effects of SDS and nanographite on hydrate formation, the formation of carbon dioxide hydrate using a pure ice powder−nitrogen-cooled system and a TBAB-only system was studied. The experiments involving different accelerators are labeled 1−12, as shown in Table 2. Except for the pure ice−nitrogen gas system, the trends in the temperature and pressure of all experiments were similar, so we discuss one representative case only. After the formation of carbon dioxide hydrate, the temperature reached the set temperature and the pressure stabilized; the overall hydrate formation time was 24 h. The temperature and pressure changes during carbon dioxide hydrate formation in the TBAB and pure ice−nitrogen gas systems are shown in Figure 2. As indicated in the figure, there are three main stages: the induced nucleation period (marked 0−A in the figure), rapid hydrate formation, and an equilibrium region.

From point 0−A in Figure 2, the temperature of the TBAB accelerator system first rises, then decreases slightly, and then rises again. In the same time period, the pure ice−nitrogen system shows a rapid increase, followed by a slight decrease in temperature. Based on these results, no significant hydrate formation occurs in this time period, which corresponds to the induced nucleation period. For the TBAB system, the point at which the temperature rises rapidly and intersects with the nitrogen temperature curve and the corresponding pressure decreases indicates the start of rapid hydrate formation. Thus, this is the hydrate-formation stage. Figure 3 shows the corresponding results for pure ice powder−nitrogen, pure ice powder−TBAB, and pure ice powder−TBAB−1.25 g/L nanographite systems. The induced nucleation periods for these last two systems are marked 0−A1 and 0−A2, respectively. From point A, massive hydrate formation starts in these systems. In Figure 2, points A−D indicate the rapid hydrate formation stage. Point C indicates the end of gas charging. In particular, from points C to D, the pressure drops sharply, indicating the formation of a large number of hydrates. In contrast, from point D to the end of the experiment, the pressure decreases slowly until it plateaus, and the reactor temperature then gradually stabilizes at 272.65 K, indicating that hydrate formation is complete.

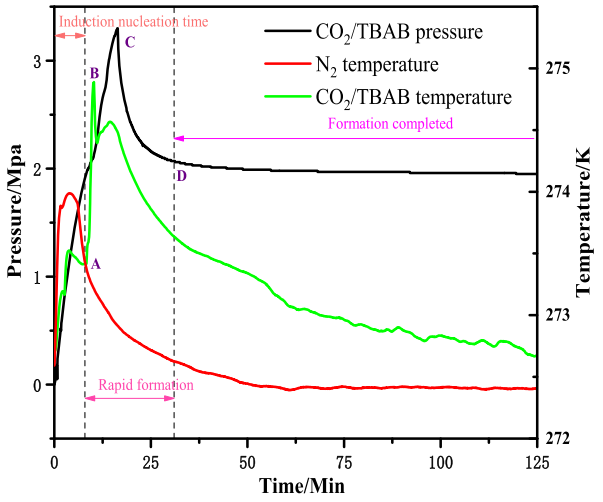

Figure 2. Temperature and pressure during the formation of carbon dioxide hydrate in the TBAB and pure ice systems.

3.2. Effect of Different Accelerator Systems in the Induction Period. Figures 4 and 5 show the induced nucleation times for hydrate formation for the different systems. As shown, the induced nucleation time for the compound systems are shorter than that of the pure ice powder system, which is consistent with the findings of Zhang et al.[29] and Zhou et al.[31] who also found that the addition of SDS and nanographite shorten the induction period for carbon dioxide

https://doi.org/10.1021/acsomega.1c06834
ACS Omega 2022, 7, 15359−15368

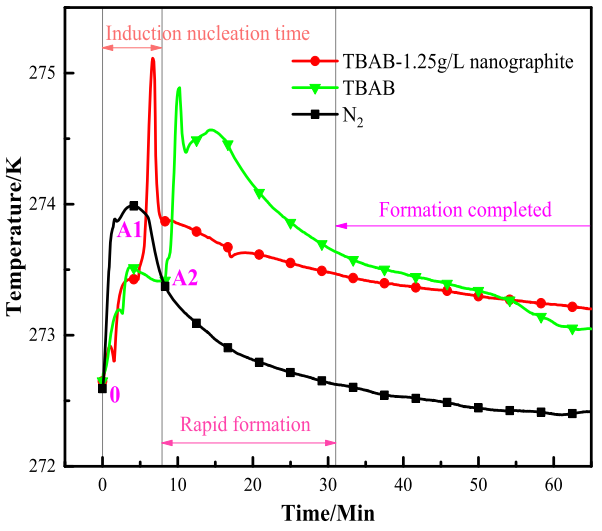

Figure 3. Temperature variation during the formation of carbon dioxide hydrate in systems containing different accelerators.

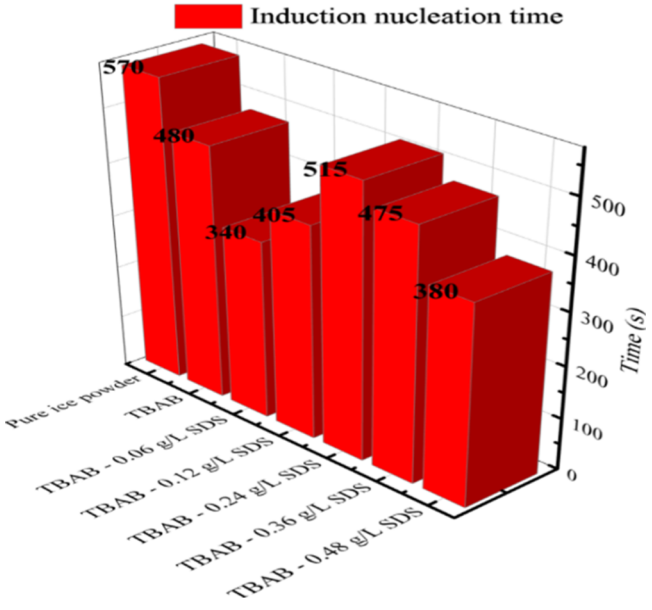

Figure 4. Induced nucleation times in the TBAB−SDS system.

hydrate formation. Crucially, there are significant differences between the induction times of the SDS and nanographite systems.

As shown in Figure 4, the induced nucleation time first increases and then decreases with increase in the SDS concentration, and the samples containing 0.06 and 0.24 g/L SDS have the shortest and longest induction times, respectively. Excluding the 0.24 g/L SDS system, all induced nucleation times of the TBAB−SDS system are shorter than that of TBAB alone, indicating that the compound accelerator enhances nucleation. Further, although higher SDS concentrations shorten the induction period, there is an optimal value.

As shown in Figure 5, for the nanographite system, the induction time decreases, then increases, and then decreases again with an increase in the nanographite concentration, and the induction times of the 2.5 and 7.25 g/L nanographite systems were the shortest and longest, respectively. The TBAB−

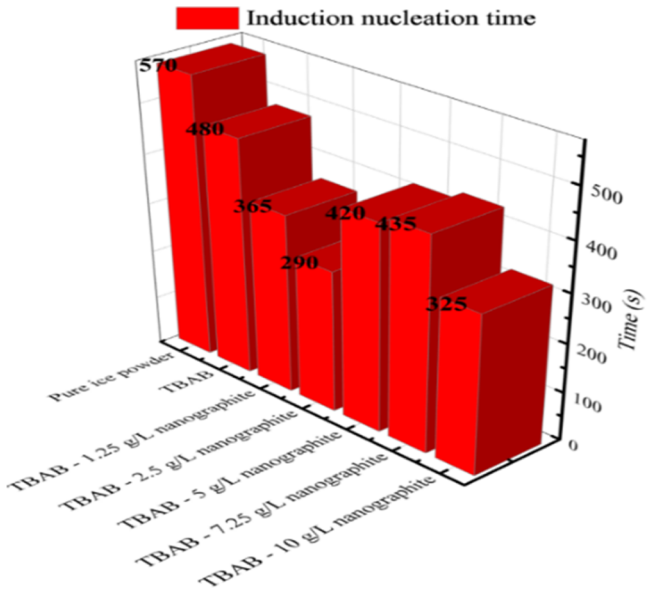

Figure 5. Induced nucleation times in the TBAB−nanographite system.

nanographite system also showed shorter nucleation times than that of TBAB alone.

In conclusion, for the compound systems, the 2.5 g/L nanographite and 0.24 g/L SDS system yielded the shortest and longest, respectively, induction times.

3.3. Effects of Different Accelerant Systems on the Production of CO_2 Hydrate. The amount of hydrate formation mainly includes the amount of gas charging process and the amount of gas hydrate formation from the stop of gas charging to the end of the formation experiment. The amount of hydrate generated during gas charging is the total amount minus that generated once gas charging stops, as shown in Table 2. The temperature and pressure at which all the experiments were conducted were 273.65 K and 3.3 MPa, respectively. During gas charging, the maximum amount of hydrate was formed for the TBAB−0.48 g/L SDS system (0.1174 mol, which accounts for 22.67% of the total amount) and the minimum amount was formed for the TBAB−0.12 g/L SDS system (0.0304 mol, which accounts for 8.21% of the total amount).

From the end of the addition of gas to the end of the experiment, the amounts of hydrate formed for cases 1−12 (Table 2) were 0.3435, 0.3457, 0.3381, 0.3397, 0.3411, 0.3359, 0.3352, 0.3358, 0.3338, 0.4048, 0.3381, and 0.3409 mol, respectively. In all cases, there was no significant difference in the amount of hydrate formed from the end of gas charging to the end of the experiments because the temperature, pressure, and ice powder quality were identical, and only the accelerators were different. Dicharry et al.[39] also found that there is little difference in the amount of hydrate formed when adding different accelerators. However, the effect of this experiment is obvious in the first 35 min of inflation stop, mainly studying the formation of the first 35 min.

The changes in the amount of hydrate formed during the course of the experiments are shown in Figures 6 and 7 for the TBAB−SDS and TBAB−nanographite systems, respectively. In these figures, 0 indicates the end of gas charging. For all systems, hydrate formation increased rapidly in the first 5−10 min. Subsequently, hydrate formation slowed and eventually plateaued. Thus, in the first 5 min, the formation rate was very low, but, with increase in time, the formation rate increased. In

https://doi.org/10.1021/acsomega.1c06834
ACS Omega 2022, 7, 15359−15368

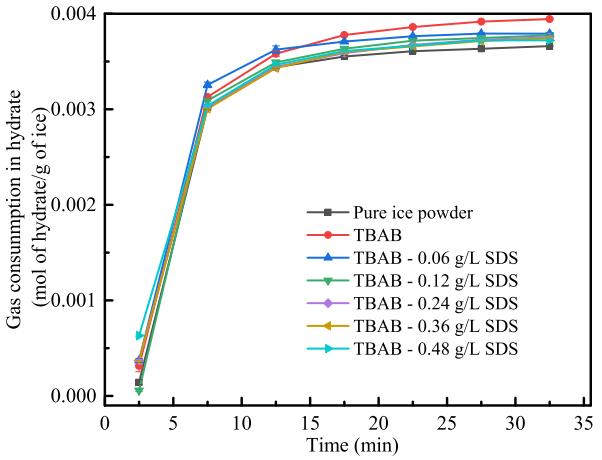

Figure 6. Amount of hydrate formed for the TBAB−SDS system at 3.3 MPa and 273.65 K.

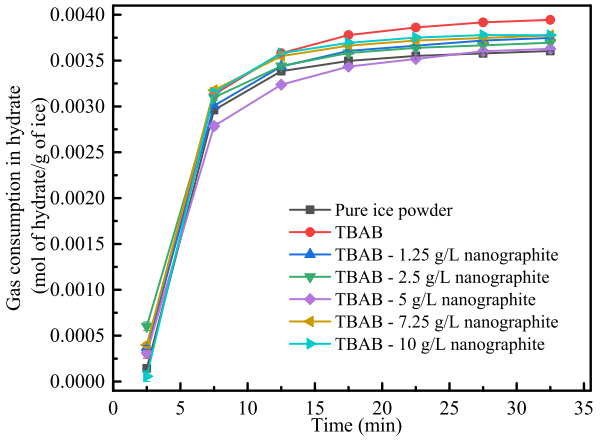

Figure 7. Amount of hydrate formed for the TBAB−nanographite system at 3.3 MPa and 273.65 K.

the later stages, the carbon dioxide consumption decreased and, thus, the formation of hydrate slowed. The average amounts of hydrate produced for the TBAB−0.48 g/L SDS and TBAB−2.5 g/L nanographite composite systems were the highest in the first 5 min after gas charging stopped. However, with an increase in time, the rate of hydrate generation decreased below those of the other systems; this is because carbon dioxide is consumed rapidly during gas charging, so a large amount of hydrate is formed, and the generation rate between 5 and 10 min is lower than those of the other systems. Over the whole course of the experiment (0−35 min), the formation rate of the TBAB-containing system was greater than that of the pure ice powder because TBAB enhances hydrate formation.[40]

As shown in Figure 6, at 0−5 min, the maximum (0.0006 mol/g) and minimum (0.0001 mol/g) amounts of hydrate were formed for the TBAB−0.48 g/L SDS and TBAB−0.12 g/L SDS systems, respectively, and there was an optimal SDS concentration. After 10 min, the maximum (0.0033 mol/g) and minimum (0.0030 mol/g) amounts of hydrate were formed for the TBAB−0.06 g/L SDS and TBAB−0.36 g/L SDS systems, respectively. Therefore, the concentration of the TBAB−SDS accelerator had a distinct effect on hydrate formation, and this effect varied over the course of the reaction.

From 0−35 min, hydrate formation in the TBAB-only system was greater than those of the TBAB−SDS systems, and the TBAB−0.06 g/L SDS and TBAB−0.48 g/L SDS systems produced the most and the least, respectively, amount of hydrate. However, both of these values are greater than that of the pure ice powder system. Therefore, the addition of SDS increased the amount of hydrate formation probably because SDS reduces the surface tension and increases the solubility of the hydrate.[41,42] However, there was no simple linear, positive correlation between the SDS concentration and hydrate formation.

As shown in Figure 7, at 0−5 min, the maximum (0.0006 mol/g) and minimum (0.0001 mol/g) amounts of hydrate were formed for the TBAB−2.5 g/L nanographite and TBAB−10 g/L nanographite systems, respectively, clearly showing that the concentration of nanographite has a significant effect on hydrate formation. As for the SDS system, the amounts of hydrate formed in the nanographite systems were greater than that formed in the pure ice powder system. At 0−35 min, the maximum amount of hydrate was formed for the TBAB−10 g/L nanographite system (0.0038 mol/g). The reason for the enhanced hydrate formation is that nanographite provides many nucleation sites, thus increasing the hydrate nucleation rate, as well as enhanced heat and mass transfer, thus promoting carbon dioxide hydrate formation.[43] The minimum hydrate formation was obtained for the TBAB−5 g/L nanographite system (0.0036 mol/g), suggesting the inhibition of hydrate formation beyond the optimal nanographite concentration.

3.4. Influence of Different Accelerator Systems on the Formation Rate of CO_2 Hydrate. The rates of hydrate formation for the different systems are shown in Figures 8 and 9.

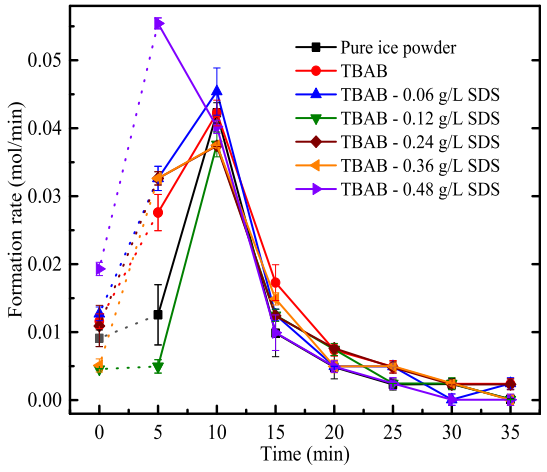

Figure 8. Rate of formation of carbon dioxide hydrate for the TBAB−SDS system at 3.3 MPa and 273.65 K.

In these figures, 0 indicates the end of gas charging, and the values indicated at 0 on the *x*-axis are the average formation rates from the beginning to the end of gas charging, that is, the average hydrate generation rate during gas charging. During gas charging, the maximum (0.019 mol/min) and minimum (0.005 mol/min) formation rates were obtained for the TBAB systems containing 0.48 and 0.12 g/L SDS, respectively, indicating again that there is an optimal SDS concentration. After gas charging, the average formation rate first increased and then decreased with an increase in the reaction time. At 0−5 min, the maximum hydrate formation rates were obtained for the TBAB systems containing 0.48 g/L SDS and 2.5 g/L nanographite. For the other systems, the formation rate

https://doi.org/10.1021/acsomega.1c06834
ACS Omega 2022, 7, 15359−15368

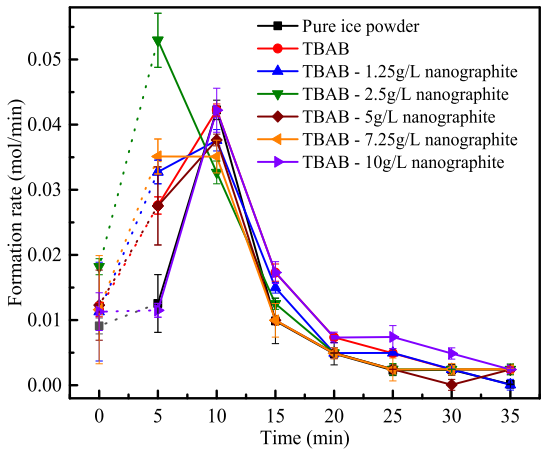

Figure 9. Rate of formation of carbon dioxide hydrate for the TBAB−nanographite system at 3.3 MPa and 273.65 K.

continued to increase, reaching their maxima 5−10 min and then decreasing. Hydrate formation is a dynamic equilibrium process, and the final formation rate of all systems fluctuates around 0 mol/min. Therefore, for the calculation of the average formation rate, we used the rates obtained at 0−35 min. Over this period, the formation rate of the TBAB-only system was higher than that of the pure ice powder system because TBAB occupies large holes or forms semi-cage hydrates so that small gas molecules can enter under relatively mild conditions, easing and accelerating hydrate formation.[26−28]

As shown in Figure 8, at 0−5 min, the maximum (0.055 mol/min) and minimum (0.005 mol/min) hydrate formation rates were obtained for the TBAB−0.48 g/L SDS and TBAB−0.12 g/L SDS systems, respectively. In this system, enhanced hydrate formation occurs because, as mentioned earlier, SDS reduces the surface tension and increases hydrate solubility, thus increasing the rate[44,45] and amount of hydrate formed.[41,42] However, below the critical micelle concentration of SDS,[46] its ability to reduce the solution surface tension and increase the gas solubility is low; thus, the rate of hydrate formation is relatively slow.[47] In contrast, above the critical micelle concentration,[46] the hydrate film is formed too quickly, thus preventing gas−liquid contact, hindering hydrate formation, and resulting in a low hydrate formation rate. At 10−35 min, the maximum and minimum hydrate formation rates were obtained for the TBAB−0.06 g/L SDS and TBAB−0.48 g/L SDS systems, respectively, but the formation rate of the pure TBAB system was greater than those of the complex systems. Other researchers have also reported differences in the hydrate formation rate over the course of reaction in systems containing TBAB and SDS. For example, Mech et al.[30] found that the hydrate formation rate in a TBAB/600 ppm SDS system was faster than that of TBAB alone in the initial 3 h, but, after 3 h, the rate was significantly slower.

As shown in Figure 9, at 0−5 min, the formation rate of all TBAB and nanographite composite systems is higher than that of the pure ice powder. The reason is that nanographite increases the nucleation rate of hydrate by providing more nucleation points for TBAB molecules. The maximum (0.053 mol/min) and minimum (0.0115 mol/min) hydrate formation rates were obtained for the TBAB−2.5 g/L nanographite and TBAB−10 g/L nanographite systems, respectively, but the rates were all greater than that of the pure ice powder system, and there was an optimal TBAB−nanographite concentration. Importantly, the relationship between the concentration and formation rate was not linear, and the effect of the concentration varied with the course of the reaction. Mekala et al.[48] found that the initial rate of carbon dioxide hydrate formation in a brine system was greater than that in a pure water system; however, after the initial stages of the reaction, the formation rate in the pure water system was greater than that of the brine system.

At 0−35 min, the maximum and minimum formation rates were obtained for the TBAB−10 g/L nanographite and TBAB−5 g/L nanographite systems, respectively. In addition, only the TBAB−10 g/L nanographite system had a higher rate of hydrate formation than TBAB alone because of the synergistic interaction of the nanographite and TBAB,[49] which improved the hydrate nucleation rate,[50−52] making this the optimal nanographite concentration.

3.5. Effects of Different Accelerant Systems on Conversion Rate. The rates of conversion of ice to CO_2 hydrate during gas charging are shown in Table 2. For the TBAB−SDS systems, the maximum (21.51%) and minimum (3.58%) conversions were obtained for the TBAB−0.48 g/L SDS and TBAB−0.12 g/L SDS systems, respectively. For the TBAB−nanographite systems, the maximum (10.36%) and minimum (7.22%) conversions were obtained for the TBAB−2.5 g/L nanographite and TBAB−10 g/L nanographite systems, respectively. Among all the complex systems, TBAB−0.48 g/L SDS and TBAB−0.12 g/L SDS had the highest and lowest conversions, respectively. The overall conversion rates for cases 1−12 in Table 2 are 50.94, 51.59, 48.31, 43.58, 51.18, 44.32, 60.98, 47.66, 49.67, 57.79, 49.71, and 47.36%, respectively.

Figures 10 and 11 show the conversion rates for all systems from the end of gas charging to the end of the experiment. In

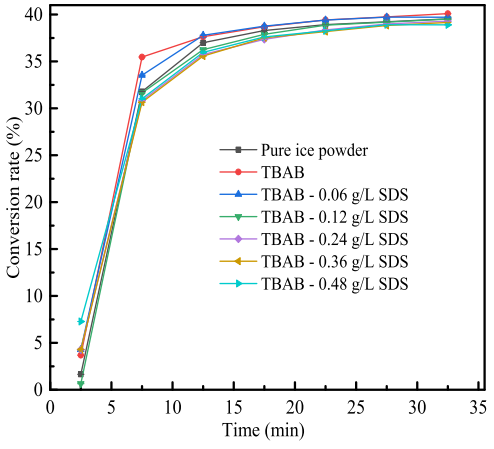

Figure 10. Conversion rates for the TBAB−SDS system at 3.3 MPa and 273.65 K.

these figures, 0 indicates the end of gas charging, the conversion of all systems increased rapidly 5−10 min and, then, increased slowly as hydrate formation slowed. At 0−5 min, the maximum conversion rates were obtained for the TBAB−0.48 g/L SDS and TBAB−2.5 g/L nanographite systems: 7.27 and 6.95%, respectively, whereas the minimum rates were obtained for the TBAB−0.12 g/L SDS and TBAB−10 g/L nanographite systems: 0.65 and 0.66%, respectively, demonstrating the differing effects of the concentrations of SDS and nanographite on hydrate formation. Thus, hydrate conversion in the initial stages is improved by the addition of the accelerators. At 0−35 min, the highest conversion rate was obtained for the TBAB−0.06 g/L SDS system, and the lowest rate was obtained for the

https://doi.org/10.1021/acsomega.1c06834
ACS Omega 2022, 7, 15359−15368

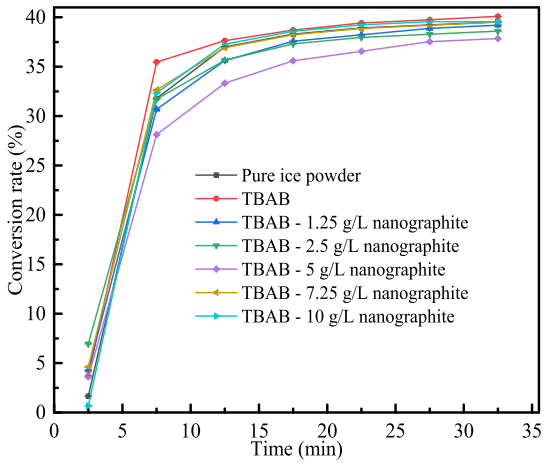

Figure 11. Conversion rates for the TBAB−nanographite system at 3.3 MPa and 273.65 K.

TBAB−0.48 g/L SDS system. For the nanographite systems, TBAB−10 g/L nanographite and TBAB−5 g/L nanographite yielded the highest and lowest conversions, respectively.

The conversion rates from the end of gas charging to the end of the experiment for cases 1−12 in Table 2 are 40.45, 40.71, 39.81, 40, 40.16, 39.55, 39.47, 39.54, 39.3, 47.66, 39.81, and 40.14%, respectively. Except for the TBAB−5 g/L nanographite system, the other composite systems yielded lower conversions than the pure ice powder system, and the conversion of the TBAB−2.5 g/L nanographite system was the lowest. Further, the conversion varied little from the end of gas charging to the end of the experiment, which is consistent with the results of Lin[52] and Ando.[53] Crucially, the addition of TBAB alone increases the conversion of the hydrate compared to that with pure ice,[54] but the use of TBAB and nanographite reduces this effect. Yu et al.[55] found that nanographite slightly inhibits the formation of carbon dioxide hydrates and affects phase equilibrium. Nashed et al.[43] reported that nanofluids do not significantly promote or inhibit hydrates, and, thus, nanomaterials are mainly used as kinetic accelerators to promote hydrate formation.

4. CONCLUSIONS

The effects of TBAB, SDS, and nanographite accelerators on the formation of carbon dioxide hydrates were studied. The effects of these compounds on hydrate formation were assessed based on the induced nucleation time, speed of hydrate formation, amount of hydrate generated, and conversion of ice to carbon dioxide hydrate. The following conclusions can be drawn.

(1) TBAB alone promoted the formation of carbon dioxide hydrates in the first 35 min after gas charging. The amounts of hydrate produced, formation rate, and ice conversion of the TBAB-only system are greater than those of the pure ice powder system, whereas the induced nucleation time is shorter than that of the pure ice powder system.

(2) The addition of TBAB with SDS or nanographite reduces the induction (nucleation) period. For the TBAB−SDS system, with an increase in the SDS concentration, the induced nucleation time first increased and then decreased, and the TBAB−0.06 g/L SDS and TBAB−0.24 g/L SDS systems yielded the shortest and longest, respectively, induction periods. For the TBAB−nanographite system, the induction time first decreased, then increased, and then decreased again with an increase in the nanographite concentration. The induced nucleation times of the TBAB−2.5 g/L nanographite and TBAB−7.25 g/L nanographite systems are the shortest and the longest, respectively. However, the induced nucleation time with TBAB alone is longer than that with TBAB−nanographite.

(3) The composite accelerators showed few differences in total hydrate production, formation rate, and conversion from the beginning of gas charging to the end of the experiment. Nevertheless, concerning these factors, the 0.48 g/L SDS and TBAB−0.12 g/L SDS systems showed the best and worst performance, respectively. The hydrate formation was the highest in the first 35 min after gas charging stopped, but these effects vary over the course of hydrate formation. In particular, the effects of the accelerators were not obvious after the end of gas charging because hydrate formation occurred at a low rate.

(4) In the first 35 min, after the end of gas charging, the 0.06 g/L SDS system produced the highest amount of hydrate and had the highest generation rate and ice conversion, whereas the 0.12 g/L SDS yielded the lowest generation amount, ice conversion, and generation rate. For the TBAB−nanographite system, these performance metrics for the 10 g/L nanographite and 5 g/L nanographite systems were the best and worst, respectively.

(5) Therefore, to generate hydrates rapidly in large amounts, TBAB is the optimal single accelerator and TBAB and 10 g/L nanographite are the best combined accelerator.

AUTHOR INFORMATION

Corresponding Author

Yingmei Wang − *Western China Research Center of Energy & Environment, Lanzhou University of Technology, Lanzhou 730050, China; Key Lab of Complementary Energy System of Biomass and Solar Energy, Lanzhou, Gansu Province 730050, China; Collaborative Innovation Center of Key Technology for Northwest Low Carbon Urbanization, Lanzhou 730050, China*; Email: wymch@lzb.ac.cn

Authors

Aili Niu − *Western China Research Center of Energy & Environment, Lanzhou University of Technology, Lanzhou 730050, China; Key Lab of Complementary Energy System of Biomass and Solar Energy, Lanzhou, Gansu Province 730050, China; Collaborative Innovation Center of Key Technology for Northwest Low Carbon Urbanization, Lanzhou 730050, China*; orcid.org/0000-0002-2968-1327

Shenghao Liu − *Western China Research Center of Energy & Environment, Lanzhou University of Technology, Lanzhou 730050, China; Key Lab of Complementary Energy System of Biomass and Solar Energy, Lanzhou, Gansu Province 730050, China; Collaborative Innovation Center of Key Technology for Northwest Low Carbon Urbanization, Lanzhou 730050, China*

Ji Chen − *State Key Laboratory of Frozen Soil Engineering, Northwest Institute of Eco-Environment and Resources, Chinese Academy of Sciences, Lanzhou 730000, China*

Xuemin Zhang − *Western China Research Center of Energy & Environment, Lanzhou University of Technology, Lanzhou 730050, China; Key Lab of Complementary Energy System of*

https://doi.org/10.1021/acsomega.1c06834
ACS Omega 2022, 7, 15359−15368

Biomass and Solar Energy, Lanzhou, Gansu Province 730050, China; Collaborative Innovation Center of Key Technology for Northwest Low Carbon Urbanization, Lanzhou 730050, China; orcid.org/0000-0002-4054-0007

Jing Zhan − *State Key Laboratory of Frozen Soil Engineering, Northwest Institute of Eco-Environment and Resources, Chinese Academy of Sciences, Lanzhou 730000, China*

Complete contact information is available at: https://pubs.acs.org/10.1021/acsomega.1c06834

Funding

This work was supported by the National Natural Science Foundation of China (no. 41661103), Open Fund of National Key Laboratory of Frozen Soil Engineering, Chinese Academy of Sciences (no. SKLFSE201406), and National Key R & D projects (no. 2017YFC0307303).

Notes

The authors declare no competing financial interest.

■ ACKNOWLEDGMENTS

Thanks to Zhaohui Zhang for helping with these experiments.

■ REFERENCES

(1) Wu, C.; Sun, C.; Yang, J.; Chen, Y.; Zhao, K. Research advances of hydrate-based technology for transport of natural gas. *Natural Gas and Oil* **2017**, *1*, 29−35.

(2) Yang, Y. B.; Xie, Y. M.; Zhuang, Y. Q.; Rui, M. A.; WANG, X. Experimental research on seawater desalination in compression refrigeration cycle system. *Fluid Mach.* **2018**, *46*, 68−72.

(3) Sun, Y.; Zhou, L.; Yue, L.; Geology, D. O. Development status of CO2 marine sequestration. *Geol. Sci. Technol. Inf.* **2018**, *37*, 212−218.

(4) Zhao, L. I.; Zhao, Y.; Fan, Y. Research progress of phase change cold storage slurry materials. *Chem. Ind. Eng. Prog.* **2018**, *37*, 108−116.

(5) Lang, X.; Fan, S.; Wang, Y. Intensification of methane and hydrogen storage inclathrate hydrate and future prospect. *J. Nat. Gas Chem.* **2010**, *19*, 203−209.

(6) Veluswamy, H. P.; Kumar, A.; Seo, Y.; Lee, J. D.; Linga, P. A review of solidified natural gas (SNG) technology for gas storage via clathrate hydrates. *Appl. Energy* **2018**, *216*, 262−285.

(7) Sloan, E. D. *Clathrate Hydrates of Natural Gases*; Marcel Dekker: New York, 2007; pp 1−9.

(8) Xia, Z.-M.; Li, X.-S.; Chen, Z.-Y.; Li, G.; Yan, K.-F.; Xu, C.-G.; Lv, Q.-N.; Cai, J. Hydrate-based CO2 capture and CH4 purification from simulated biogas with synergic additives based on gas solvent. *Appl. Energy* **2016**, *162*, 1153−1159.

(9) Babaee, S.; Hashemi, H.; Mohammadi, A. H.; Naidoo, P.; Ramjugernath, D. Kinetic study of hydrate formation for argon + TBAB + SDS aqueous solution system. *J. Chem. Thermodyn.* **2018**, *116*, 121−129.

(10) Behzad, P.; Sabil, K. M.; Kok, K. L.; Bhajan, L.; Khashayar, N. Production of gas hydrate in a semi-batch spray reactor process as a means for separation of carbon dioxide from methane. *Chem. Eng. Res. Des.* **2018**, *138*, 168−175.

(11) Ni, L.; Lc, A.; Cl, A.; Liang, Y. A.; Dl, A. Experimental study of carbon dioxide hydrate formation in the presence of graphene oxide. *Energy* **2020**, *211*, 118994−118997.

(12) Cai, J.; Xu, C.; Xia, Z.; Chen, Z.; Li, X. Hydrate-based methane separation from coal mine methane gas mixture by bubbling using the scale-up equipment. *Appl. Energy* **2017**, *105*, 4983−4989.

(13) Zhong, D.-L.; He, S.-Y.; Sun, D.-J.; Yang, C. Comparison of methane hydrate formation in stirred reactor and porous media in the presence of SDS. *Energy Procedia* **2014**, *61*, 1573−1576.

(14) Foroutan, S.; Mohsenzade, H.; Dashti, A.; Roosta, H. Comparison of kinetic inhibition of ethylene and methane hydrate formation when pegs with low and high molecular weights meet common KHIs. *Fuel* **2020**, *276*, 118029−118111.

(15) Yu, Y.-S.; Zhang, Q.-Z.; Li, X.-S.; Chen, C.; Zhou, S.-D. Kinetics, compositions and structures of carbon dioxide/hydrogen hydrate formation in the presence of cyclopentane. *Appl. Energy* **2020**, *265*, 114808−114812.

(16) Xu, N.; Liu, Y.; Cheng, Z.; Wang, S.; Jiang, L.; Song, Y. Morphology-Based Kinetic Study of the Formation of Carbon Dioxide Hydrates with Promoters. *Energy Fuels* **2020**, *34*, 7307−7315.

(17) Katipot, I.; Pramoch, R.; Santi, K. Effects of temperature and pressure on the methane hydrate formation with the presence of tetrahydrofuran (THF) as a promoter in an unstirred tank reactor. *Fuel* **2019**, *255*, 115705.

(18) Abedi-Farizhendi, S.; Rahmati-Abkenar, M.; Manteghian, M.; Salehzadeh Yekshaveh, J.; Zahmatkeshan, V. Kinetic study of propane hydrate in the presence of carbon nanostructures and SDS. *J. Pet. Sci. Eng.* **2019**, *172*, 636−642.

(19) Nashed, O.; Partoon, B.; Lal, B.; Sabil, K. M.; Shariff, A. M. Investigation of functionalized carbon nanotubes' performance on carbon dioxide hydrate formation. *Energy* **2019**, *174*, 602−610.

(20) Pahlavanzadeh, H.; Javidani, A. M.; Ganji, H.; Mohammadi, A. Investigation of the effect of NaCl on the kinetics of R410a hydrate formation in the presence and absence of cyclopentane with potential application in hydrate-based desalination. *Ind. Eng. Chem. Res.* **2020**, *59*, 14115−14125.

(21) Kawasaki, T.; Obara, S. CO2 hydrate heat cycle using a carbon fiber supported catalyst for gas hydrate formation processes. *Appl. Energy* **2020**, *269*, 115125.

(22) Farhang, F.; Nguyen, A. V.; Hampton, M. A. Influence of sodium halides on the kinetics of CO2 hydrate formation. *Energy Fuels* **2014**, *28*, 1220−1229.

(23) Liu, W.; Li, Y.; Xu, X. Influence factors of methane hydrate formation from ice: temperature, pressure and SDS surfactant. *Chin. J. Chem. Eng.* **2019**, *27*, 405−410.

(24) He, Y.; Sun, M.-T.; Chen, C.; Zhang, G.-D.; Chao, K.; Lin, Y.; Wang, F. Surfactant-based promotion to gas hydrate formation for energy storage. *J. Mater. Chem. A* **2019**, *7*, 21634−21661.

(25) Liu, Z.; Pan, Z.; Zhang, Z.; Liu, P.; Shang, L.; Li, B. Effect of porous media and sodium dodecyl sulphate complex system on methane hydrate formation. *Energy Fuels* **2018**, *32*, 5736−5749.

(26) Ye, N.; Zhang, P.; Liu, Q. S. Kinetics of hydrate formation in the CO2+TBAB+H2O system at low mass fractions. *Ind. Eng. Chem. Res.* **2014**, *53*, 10249−10255.

(27) Babu, P.; Chin, W. I.; Kumar, R.; Linga, P. Systematic evaluation of tetra-n-butyl ammonium bromide (TBAB) for carbon dioxide capture employing the clathrate process. *Ind. Eng. Chem. Res.* **2014**, *53*, 4878−4887.

(28) Nguyen, N. N.; Nguyen, A. V.; Nguyen, K. T.; Rintoul, L.; Dang, L. X. Unexpected inhibition of CO2 gas hydrate formation in dilute TBAB solutions and the critical role of interfacial water structure. *Fuel* **2016**, *185*, 517−523.

(29) Zhang, F.; Wang, X.; Lou, X.; Lipiński, W.; Kaiser, M. J. The effect of sodium dodecyl sulfate and dodecyltrimethylammonium chloride on the kinetics of CO2 hydrate formation in the presence of tetra-n-butyl ammonium bromide for carbon capture applications. *Energy* **2021**, *227*, 120424−120444.

(30) Mech, D.; Gupta, P.; Sangwai, J. S. Kinetics of methane hydrate formation in an aqueous solution of thermodynamic promoters (THF and TBAB) with and without kinetic promoter (SDS). *J. Nat. Gas Sci. Eng.* **2016**, *35*, 1519−1534.

(31) Zhou, S.; Jiang, K.; Zhao, Y.; Chi, Y.; Wang, S.; Zhang, G. Experimental investigation of CO2 hydrate formation in the water containing graphite nanoparticles and tetra-n-butyl ammonium bromide. *J. Chem. Eng. Data* **2018**, *63*, 389−394.

(32) Babaee, S.; Hashemi, H.; Mohammadi, A. H.; Naidoo, P.; Ramjugernath, D. Kinetic study of hydrate formation for argon+TBAB +SDS aqueous solution system. *J. Chem. Thermodyn.* **2018**, *116*, 121−129.

(33) Sarlak, H.; Azimi, A.; Mostafa, S.; Ghomshe, T.; Mirzaei, M. ECC Effect of TBAB and SDS surfactants on the interfacial tension of CO2 Hydrate in water. *Eurasian Chem. Commun.* **2019**, *2*, 319−328.

(34) Zhou, S. D.; Yu, X. W.; Li, Q. L.; Li, L. Effect of the combination of nano graphite particles and SDS on hydrate formation characteristics. *Nat. Gas Chem. Ind.* **2017**, *42*, 50−53.
(35) Lin, Z.; Zhou, S.; Wang, S.; Lei, W.; Li, J. Surfactant surface tension effects on promoting hydrate formation: an experimental study using fluorocarbon surfactant (Intechem-01) + SDS composite surfactant. *J. Environ. Prot.* **2013**, *4*, 42−48.
(36) Sun, D.; Englezos, P. Storage of CO2 in a partially water saturated porous medium at gas hydrate formation conditions. *Int. J. Greenhouse Gas Control* **2014**, *25*, 1−8.
(37) Li, X.-S.; Zhang, Y.; Li, G.; Chen, Z.-Y.; Yan, K.-F.; Li, Q.-P. Gas hydrate equilibrium dissociation conditions in porous media using two thermodynamic approaches. *J. Chem. Thermodyn.* **2008**, *40*, 1464−1474.
(38) Smith, J. M.; Vanness, H. C.; Abbott, M. M. Introduction to chemical engineering thermodynamics. *J. Chem. Educ.* **1950**, *27*, 584.
(39) Dicharry, C.; Diaz, J.; Torré, J.-P.; Ricaurte, M. Influence of the carbon chain length of a sulfate-based surfactant on the formation of CO2, CH4 and CO2-CH4 gas hydrates. *Chem. Eng. Sci.* **2016**, *152*, 736−745.
(40) Li, D.-L.; Sheng, S.-M.; Zhang, Y.; Liang, D.-Q.; Wu, X.-P. Effects of multiwalled carbon nanotubes on CH4 hydrate in the presence of tetra-n-butyl ammonium bromide. *RSC Adv.* **2018**, *8*, 10089−10096.
(41) Brown, E. P.; Koh, C. A. Micromechanical measurements of the effect of surfactants on cyclopentane hydrate shell properties. *Phys. Chem. Chem. Phys.* **2016**, *18*, 594−600.
(42) Liu, Z.; Li, Y.; Wang, W.; Song, G.; Lu, Z.; Ning, Y.; Liu, S. Experimental investigation on the micro-morphologies and growing process of methane hydrate formation in SDS solution. *Fuel* **2021**, *293*, 120320−120326.
(43) Nashed, O.; Partoon, B.; Lal, B.; Sabil, K. M.; Shariff, A. M. Review the impact of nanoparticles on the thermodynamics and kinetics of gas hydrate formation. *J. Nat. Gas Sci. Eng.* **2018**, *55*, 452−465.
(44) Lin, W.; Chen, G.-J.; Sun, C.-Y.; Guo, X.-Q.; Wu, Z.-K.; Liang, M.-Y.; Chen, L.-T.; Yang, L.-Y. Effect of surfactant on the formation and dissociation kinetic behavior of methane hydrate. *Chem. Eng. Sci.* **2004**, *59*, 4449−4455.
(45) Toshiyuki, K.; Katsumi, K.; Kenji, T.; Tohko, A.; Atsushi, N.; Yasuhide, M.; Minoru, H. Pharmacological profile of naldemedine, a peripherally acting μ-opioid receptor antagonist: comparison with naloxone and naloxegol. *J. Pharmacol. Exp. Ther.* **2020**, *373*, 438−444.
(46) Zhang, L.; Wang, S.; Zhou, S.; Cai, D.; Wang, L. Research progress in surfactant effects on promoting gas hydrate formation. *Chin. J. Appl. Chem.* **2014**, *31*, 505−512.
(47) Yu, H. J.; Wang, S. L.; Jiang, G. S.; Zhang, H. J.; Yu, Y. T. Experimental study on the effect of surfactant on the formation of CO2 hydrate. *Nat. Sci.* **2011**, *23*, 55−59.
(48) Mekala, P.; Babu, P.; Sangwai, J. S.; Linga, P. Formation and dissociation kinetics of methane hydrates in seawater and silica sand. *Energy Fuels* **2014**, *28*, 2708−2716.
(49) Zarenezhad, B. Accurate prediction of the interfacial tension of surfactant/fluid mixtures during gas hydrate nucleation: The case of SDS surfactant-based systems near ethylene hydrate formation region. *J. Mol. Liq.* **2014**, *191*, 161−165.
(50) Yegya Raman, A. K.; Koteeswaran, S.; Venkataramani, D.; Clark, P.; Bhagwat, S.; Aichele, C. P. A comparison of the rheological behavior of hydrate forming emulsions stabilized using either solid particles or a surfactant. *Fuel* **2016**, *179*, 141−149.
(51) Lianga, P.; Clarke, M. A. A review of reactor designs and materials employed for increasing the rate of gas hydrate formation. *Energy Fuels* **2017**, *31*, 1−13.
(52) Lin, W.; Chen, G.-J.; Sun, C.-Y.; Guo, X.-Q.; Wu, Z.-K.; Liang, M.-Y.; Chen, L.-T.; Yang, L.-Y. Effect of surfactant on the formation and dissociation kinetic behavior of methane hydrate. *Chem. Eng. Sci.* **2004**, *59*, 4449−4455.
(53) Ando, N.; Kuwabara, Y.; Mori, Y. H. Surfactant effects on hydrate formation in an unstirred gas/liquid system: An experimental study using methane and micelle-forming surfactants. *Chem. Eng. Sci.* **2012**, *73*, 79−85.
(54) Yang, M.; Zhou, H.; Wang, P.; Song, Y. Effects of additives on continuous hydrate-based flue gas separation. *Appl. Energy* **2018**, *221*, 374−385.
(55) Yu, Y.-s.; Zhou, S.-d.; Li, X.-s.; Wang, S.-l. Effect of graphite nanoparticles on CO2 hydrate phase equilibrium. *Fluid Phase Equilib.* **2016**, *414*, 23−28.

https://doi.org/10.1021/acsomega.1c06834
ACS Omega 2022, 7, 15359−15368